JOURNAL OF GEOPHYSICAL RESEARCH, VOL. 101, NO. C11, PAGES 25,599–25,614, NOVEMBER 15, 1996

Monsoon/El Nino–Southern Oscillation relationships in a simple coupled ocean-atmosphere model

Ilana Wainer
Department of Physical Oceanography, University of São Paulo, São Paulo, Brazil

Peter J. Webster
Program in Atmospheric and Oceanic Sciences, University of Colorado at Boulder

Abstract. A coupled ocean-atmosphere model is used to investigate the equatorial Indian and Pacific Oceans' response to the seasonally varying monsoon winds and the relationship between monsoon variations and the El Niño–Southern Oscillation phenomenon (ENSO). The atmosphere is a simple linear shallow water system driven by a mass source/sink term that is proportional to the sea surface temperature (SST) over the oceans and the heat balance over land. The ocean is modeled using the *Anderson and McCreary* [1985] reduced-gravity transport model driven by atmospheric wind stress forcing and a parameterized heat flux. The model domain includes both the Indian and Pacific Oceans and land masses to represent Asia and Africa. Results show that variations in the model's monsoon circulation (evolving somehow from other influences) induce changes in the large-scale circulation associated to ENSO. In this way the year-to-year differences in the monsoon impact on the longer-period, coupled ocean-atmosphere dynamics of the near-equatorial Pacific basin. By changing the amplitude of the monsoon forcing the interval between ENSO-like warm events varies, while the variability in the annual cycle over the Indian Ocean is hardly affected.

1. Introduction

The social and economic ramifications of the lack of precipitation over Asia have prompted considerable effort toward finding a reliable climate predictor for the monsoons. Since the time *Walker and Bliss* [1930] revealed the seesaw relationship of the meteorological variables associated with the Southern Oscillation (SO), research to establish its link to monsoon rainfall has been extensive.

At the same time the study of the El Niño–Southern Oscillation (ENSO) phenomenon has been the subject of growing interest and concern among scientists. The increased number of observational and numerical investigations on the subject leaves little doubt that interactions between the ocean and the atmosphere are at the heart of the problem as first suggested by *Bjerknes* [1969].

Yang [1990] gives an overview of the observational research that has been conducted to correlate ENSO to monsoon rainfall. In particular, he describes the studies of *Shukla and Paolino* [1983] and *Pant and Parthasaraty* [1981] that show that the warm events are inversely correlated with Indian monsoon rainfall. *Angell* [1981] also found that the warm events are preceded by periods of less rainfall and that periods of more rainfall follow the tropical Pacific warm episodes. The relationship between ENSO episodes and monsoon rainfall is inconclusive. We first note the unreliable nature of precipitation as an indicator of monsoon activity, since precipitation over Asia has a strong regional dependency. Warm events can be highly correlated with lack of precipitation over India, but in nearby Sri Lanka, warm events can be correlated with abundant rainfall, as pointed out by *Rasmusson and Carpenter* [1983]. Global analyses of sea level pressure done by *Barnett* [1984] have suggested that the Indian Ocean region may play a less passive role in the evolution of the ENSO cycle. The observational study of *Yasunari* [1990] seems to agree with this idea that changes in the monsoon may indicate, or signal, changes in ENSO.

Observational results so far [e.g., *Shukla and Paolino*, 1983; *Rasmusson and Carpenter*, 1983; *Ropelewski and Halpert*, 1987] have not shown a conclusive link between ENSO and the Indian monsoon. Shukla and Paolino find a good correlation for extreme events but weak correlation when the events are moderate. These extremes correspond to the minimum or maximum value of the Southern Oscillation Index (SOI).

Ropelewski and Halpert [1987] show more precipitation over India during cold events (SOI positive values) and less precipitation during warm events (negative SOI values). *Rasmusson and Carpenter* [1983] note the difficulty of using precipitation as a measure of monsoon strength because of its regional distribution. They find a good correlation between warm events and lack of precipitation over India. However, the precipitation in nearby Sri Lanka is abundant for the same warm event. What is the direction of the monsoon-ENSO interaction? How does the monsoon affect ENSO?

The Southern Oscillation Index is a good indicator of the aperiodicity associated with the joint variability of the Indo-Pacific Ocean region. Aperiodicity occurs in some models but not in others. *Cane and Zebiak* [1987] try to explain the aperiodicity in their coupled model in terms of internal wave dynamics. But the cause-effect relationship for the irregularity of their ENSO cycle is not clear. *Anderson and McCreary* [1985] (hereafter AM) point out that a key ingredient for the low-frequency oscillation in the Pacific Ocean is the convection in

Paper number 96JC00670.
0148-0227/96/96JC-00670$09.00

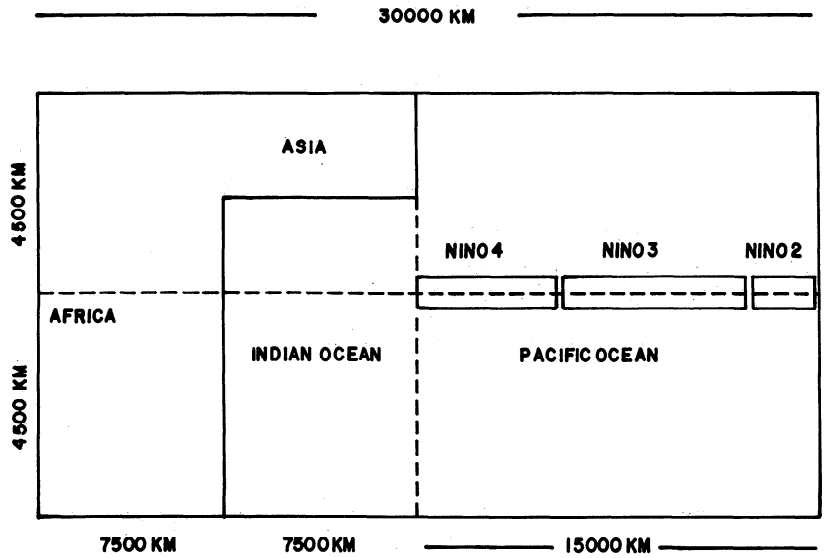

Figure 1. Schematic diagram of the model domain. The atmosphere is cyclic in longitude and extends for 30,000 km. The square continental regions simulate the African and Asian continents. There are two oceans: a model Pacific Ocean that extends for 15,000 km and a model Indian Ocean that is half that size. The two basins are bounded by an infinitesimal wall.

the west. Furthermore, they suggest that the atmospheric heating over land may fundamentally influence events over the Pacific Ocean, but, even so, their ENSO-like fluctuations are very regular. What causes the irregular period in the ENSO cycle? What are the necessary physics involved in reproducing aperiodic events?

In order to answer the questions raised above, it will be hypothesized that the monsoon onset and the ensuing localized heating over South Asia set the variability of the ocean-atmosphere system. In this way the year-to-year differences in the monsoon, coupled to the longer-period near-equatorial ocean dynamics of the Pacific basin, produce the aperiodic interannual timescale of ENSO.

It will be argued that the ENSO cycle cannot be fully described and understood without considering the Indian and Pacific Oceans simultaneously. To expand this idea, a series of simulations are conducted that indeed suggest that coupled ocean-atmosphere models should be developed with the inclusion of the strong seasonal cycle associated with the monsoon circulation over Asia.

The organization of this paper is as follows: The numerical model is described in section 2. In section 3 the results to three different numerical experiments are shown. These are discussed in section 4, while the conclusions are presented in section 5.

2. Coupled Model Formulation

The coupled model structure follows the overall design of AM, with the exception of the atmospheric component that was specifically modified to simulate the effects of the Asian monsoon cycle via a prescribed heating function. The atmosphere is a linear, shallow water perturbation model representing an "evolving" steady state atmosphere linearized about a zero basic state. A schematic of the model domain is shown in Figure 1.

The global atmosphere lies over two rectangular oceans that represent the Pacific Ocean and the Indian Ocean. The Indian Ocean is surrounded by land masses on its northern and western sides which represent the zonally asymmetric land masses of Asia and Africa.

The two oceans are separated by a solid boundary. Physically, the Indian and Pacific Oceans extend longitudinally 7500 and 15,000 km.

The sea surface temperature (SST), to which the atmosphere is coupled, is predicted by the ocean model. This SST and the heating function over land force the atmosphere.

The ocean is represented by a reduced-gravity, nonlinear, transport model which is driven by wind stress and by a *Haney* [1971] -type parameterized heat flux.

2.1. Model Atmosphere

The equations for the model atmosphere are

$$-\beta y V = -P_x - \varepsilon U \tag{1}$$

$$\beta y U = -P_y - \varepsilon V \tag{2}$$

$$c^2(U_x + V_y) = Q_T - \varepsilon P \tag{3}$$

$$Q_T = Q_O + Q_L \tag{4}$$

where U and V are the zonal and meridional components of the wind and P is the geopotential. Q_T is the heating of the atmosphere, c is the speed of a Kelvin wave, equal to 60 m s^{-1}, and ε is the coefficient of Newtonian cooling, equal to 3×10^{-5} s^{-1}. These values of ε and c are the same used by *Gill* [1980] and AM. For these choices an equatorial Kelvin wave will be damped on a length scale of $c/\beta \approx 2000$ km, while the lowest-order Rossby wave will decay on the scale of 1/3 that value $\approx$700 km.

Q_O, the latent heat release over the oceans, is related to SST according to

$$Q_O = Q_o \frac{\mathrm{SST} - (\mathrm{SST})_C}{(\mathrm{SST})_{\mathrm{EQ}} - (\mathrm{SST})_C} \Delta[\mathrm{SST} - (\mathrm{SST})_C] \tag{5}$$

where Q_o is an amplitude factor equal to 0.05 $m^2 s^{-3}$, $(SST)_{EQ}$ is the temperature calculated at the equator, and Δ is the Heaviside step function.

The strength of the forcing is proportional to the amount the model predicted SST is above some critical level $(SST)_C$ and is zero when SST is below $(SST)_C$. $(SST)_C = (SST)_{EQ} - 1.5°C$. The sensitivity of results to these choices is discussed by AM.

Q_L, the atmospheric heating over land is a function of time T and latitude ϕ according to

$$Q_L(T, \phi) = f(T)[f_1(\phi) + f_2(\phi)] \quad (6)$$

$$f_1(\phi) = A \sin(2\pi\phi/W1) \quad (7)$$

$$f_2(\phi) = B \sin(\pi\phi/W2) \quad (8)$$

$$f(T) = S - \langle S \rangle \quad (9)$$

$$S = (\pi/2) \sin\delta + \cos\delta \quad (10)$$

$$\langle S \rangle = \frac{1}{360} \int_T S dt \quad (11)$$

The structure of Q_L for the months of January (Figure 2a) and July (Figure 2b) can be seen in Figure 2. Negative (positive) contours represent heating (cooling). The continental boundaries are marked. Here f_1 represents the heating over the model African continent and f_2 the heating over model Asia. A and B are amplitude factors such that the monsoon has a maximum amplitude heating equivalent to 500 W m^{-2}. $W1$ and $W2$ are the width of the continental regions. Here $\delta = \alpha \sin(2\pi d/360)$ gives the time dependence, $\alpha = 0.23$. In longitude, f_1 and f_2 are forced to have a maximum value at the center of the continental regions and decay linearly toward the continental edge. The number of days (d) in a model year was set to be 360 for simplicity.

As noted by AM, (1)–(3) describe the response of the first baroclinic mode of the atmosphere [*Gill*, 1980] and as such assume that the main atmospheric forcing is a result of tropical convection. Other assumptions inherent to this model are that the atmospheric response to convection is linear and that convection depends only on the local SST. The first assumption can be true in the case of weak convection but untrue if the convection is strong. The latter is not entirely true since convection is also a function of surface fluxes and moisture advection.

Solutions to (1)–(3) are found by Fourier transforming the equations in x and then solving for a single equation in $\hat{V}$ (the Fourier transform of V). The $\hat{V}$ equation in finite difference form can be reduced to a tridiagonal matrix equation which is then solved: The solution is obtained by finding the inverse transforms of $\hat{V}$ and the inverse transform $\hat{U}$ and $\hat{P}$ (the Fourier transforms of U and P which can be expressed in terms of $\hat{V}$). The horizontal resolution is 150 km and is cyclic in x. The domain extends from the equator to 4500 km north and south.

2.2. Model Ocean

The equations for the model ocean, from AM, are

$$(hu)_t + (huu)_x + (huv)_y - \beta y h v = -p_x + \frac{\tau_x}{\rho} + \nu_h \nabla^2(hu) \quad (12)$$

$$(hv)_t + (huv)_x + (hvv)_y + \beta y h u = -p_y + \frac{\tau_y}{\rho} + \nu_h \nabla^2(hv) \quad (13)$$

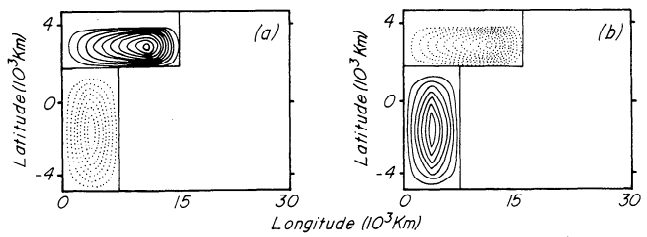

Figure 2. Land-heating Q_L for the months of (a) January and (b) July.

$$h_t + (hu)_x + (hu)_y = \frac{2\delta}{hT} - W + \gamma\left(\frac{T - T^*}{T}\right) \quad (14)$$

$$T_t + uT_x + vT_y = \frac{2}{h}\left[-\gamma(T - T^*) - \frac{\delta}{h}\right] + \nu_h \nabla^2(T) \quad (15)$$

where $g' = (\rho_{bot} - \rho_{top}/\rho_{bot})\, g$, $P = 0.5\rho\alpha g' h^2 T$ is the potential energy, and T is the temperature excess of the surface layer over the bottom layer. Here ρ, $\alpha = 0.0003°C^{-1}$ and $\nu_h = 2 \times 10^3$ m^2 s^{-1} are the density, thermal expansion coefficient and horizontal viscosity coefficient. The values of these constants are the same used by AM. Here h is the thickness of the upper layer.

The surface stresses (τ_x, τ_y) are related to the atmospheric fields according to

$$\tau_x = \rho_{atm} C'_D U \quad (16)$$

$$\tau_y = \rho_{atm} C'_D V \quad (17)$$

where C'_D has the value of 0.008 m s^{-1}. U and V are defined by the model atmosphere. The heat flux into the ocean, $Q_S = -\rho C_P \gamma(T - T^*)$, as suggested by *Haney* [1971], acts as a heat source for the layer since in this model T is always less than T^*. T^* is a function of latitude with a maximum value of 11.33°C at the equator, decreasing to 4°C at a distance of 4500 km north and south of the equator.

The finite difference versions of (12)–(15) are solved using a centered difference scheme with a time step of 1/8 day on an Arakawa C grid where T values are stored at h points. The equations are forward differenced in time once every 10 days to prevent time splitting. The model grid size is 150 km in both latitude and longitude. Kelvin waves are damped along the northern and southern boundaries to avoid contamination of the interior solution. The damping term is set to be maximum at the boundary and zero 450 km away, as it was set by AM. The reader is referred to AM for more details on the formulation of the ocean model and its sensitivity to parameters.

Some discrepancies between the model results and observations have been noted. In particular, the model's warm events do not show the typical coastal warming prior to the development of the warming in the central Pacific. As a matter of fact the SST disturbances in this model are seen only to propagate from west to east. Nonetheless, the model proved to be suitable for studying the effect of the monsoon on ENSO cycles.

3. Results

The relationship between variations in the summer monsoon and the interannual variability associated with ENSO in the Pacific Ocean is examined through a number of 100-year sim-

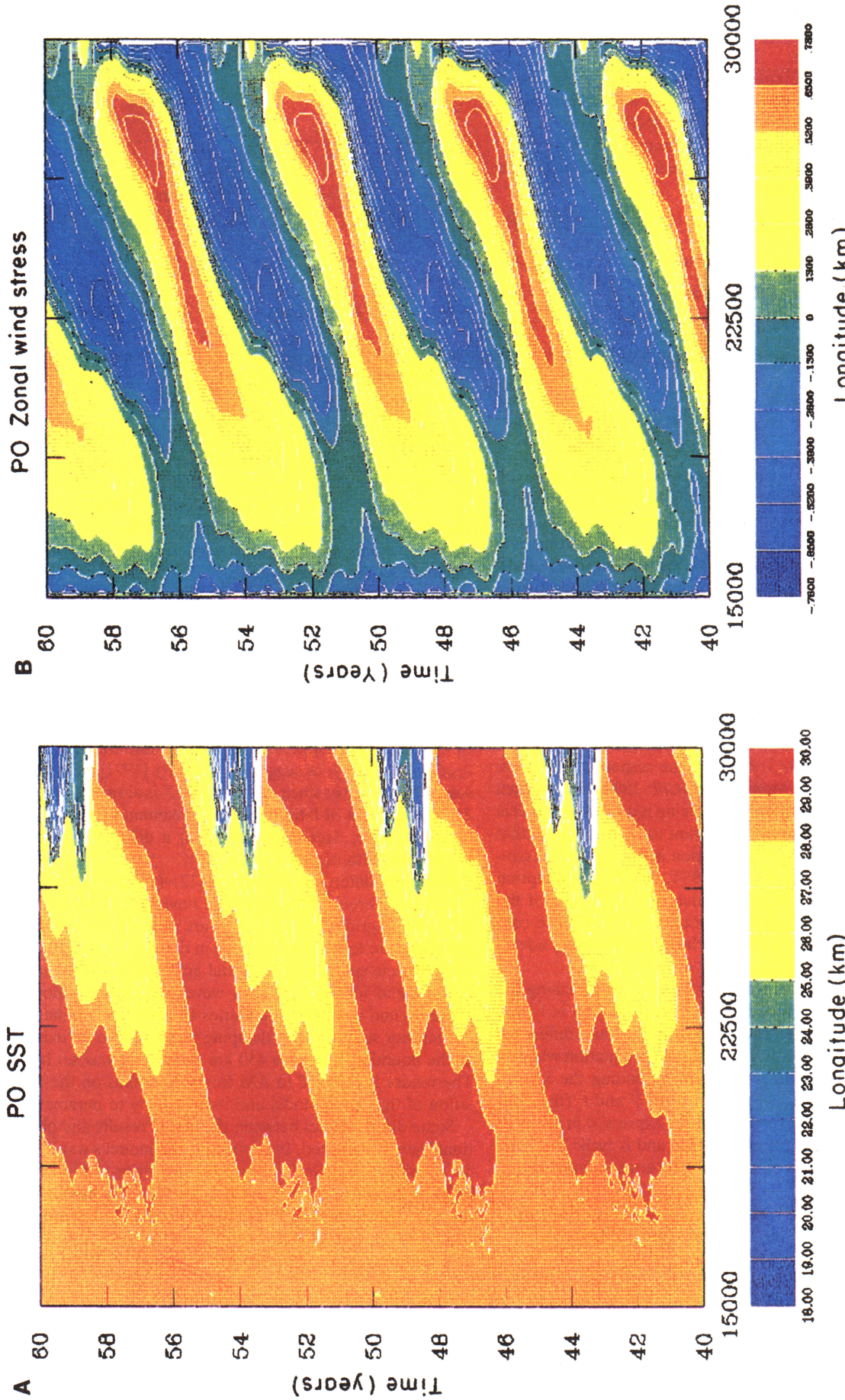

Plate 1. (a) Time versus longitude distribution of the model Pacific Ocean (PO) sea surface temperature (SST) (degrees Celsius) along the equator for RUN1 (strong monsoon). Time goes from the bottom up. The color code on the bottom of the plate has colder temperatures in the blue side of the spectrum. Warmer temperatures are related to the orange-like colors. (b) Time versus longitude distribution of the model Pacific Ocean τ_x (dynes per square centimeter) along the equator for RUN1. Negative values (easterlies) are in the blue-green side of the spectrum, while positive values (westerlies) lie on the yellow-red side.

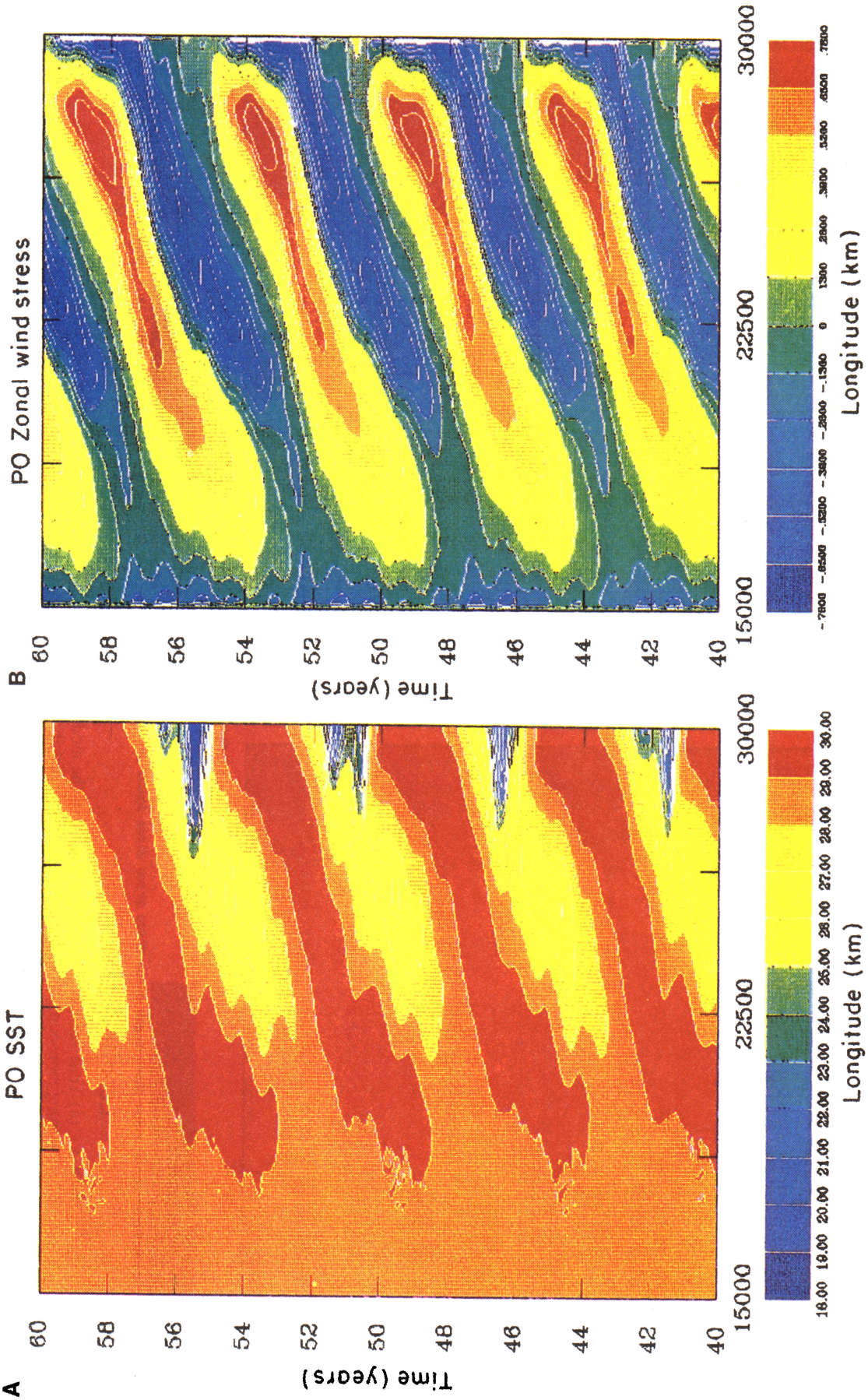

Plate 2. (a) Time versus longitude distribution of the model Pacific Ocean SST (degrees Celsius) along the equator for RUN2 (weak monsoon). Time goes from the bottom up. The color code on the bottom of the figure has colder temperatures in the blue side of the spectrum. Warmer temperatures are related to the orange-like colors. (b) Time versus longitude distribution of the model Pacific Ocean τ_x (dynes per square centimeter) along the equator for RUN2. Negative values (easterlies) are in the blue-green side of the spectrum, while positive values (westerlies) lie on the yellow-red side.

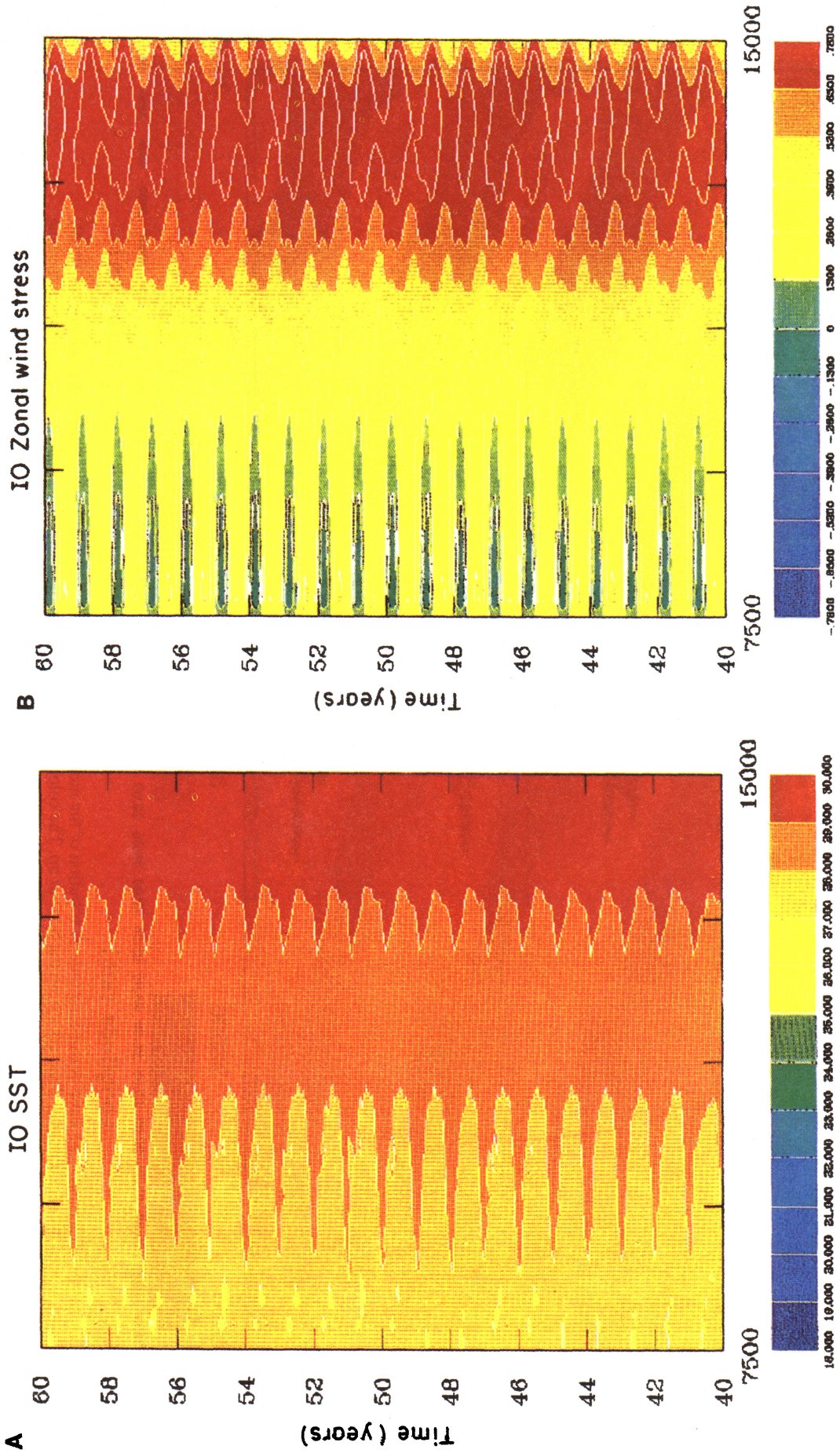

Plate 3. (a) Time versus longitude distribution of the model Indian Ocean (IO) SST (degrees Celsius) along the equator for RUN1 (strong monsoon). (b) Time versus longitude distribution of the model Indian Ocean τ_x (dynes per square centimeter) along the equator for RUN1.

ulations. The simulations fall into two categories: strong monsoon (RUN1) and weak monsoon (RUN2). The difference between their amplitude is set at 10%, which is based on the (National Meteorological Center, NMC) observed monthly mean outgoing longwave radiation (OLR) for the period between 1974 and 1988, shown by *Webster and Yang* [1992].

OLR maximum and minimum values are taken to be related to atmospheric convective minima and maxima, respectively. Low values of OLR are associated with regions of latent heat release and thus atmospheric heating and maximum precipitation. High values represent little or no latent heat release to the atmosphere. A more comprehensive analysis of the use of OLR data to identify atmospheric convective zones is given by *Webster and Yang* [1992].

In the last simulation (RUN3) the amplitude of the monsoon heating is coupled to a stochastic function in order to introduce interannual variability into the monsoon circulation. This is done by adding a random number generator function based on the seasonal variability of OLR along 90°E averaged between 10° and 20°N to the amplitude term B of (8).

The characteristics of the interannual variability of the Pacific Ocean and Indian Ocean are compared. Initially, we look at the time versus longitude plots of model Pacific Ocean SST (degrees Celsius) and zonal wind stress (τ_x, in dynes per square centimeter) along the equator in Plates 1 and 2 for the strong (RUN1) and weak (RUN2) monsoon case. Time increases along the ordinate. Only 20 years are presented of the 100-year simulation in the interest of clarity. In the SST plots (Plates 1a and 2a), maximum temperatures greater than 29°C are represented by the dark red.

The most striking characteristic of Plate 1a is the interannual propagation of the warm SST from west to east. Even though the annual cycle is part of the variability observed in the Pacific Ocean, it is the interannual changes that are the dominant signal. Note, however, that the annual cycle is more pronounced during the cold phase in the eastern Pacific Ocean. An east-west temperature gradient is evident. The warm red patches are associated with convection in the atmosphere and with a deep mixed layer (not shown). The distribution has higher SST to the west and lower SST in the east during cold years and is reversed during warm years. The propagation of the highest SST from west to east occurs at periodic intervals of 5 years. Regions of easterly and westerly wind stress anomaly exist east and west of the warm patch, respectively (Plate 1b). Again, it is noted that the westerly wind stress anomaly (positive values) originates in the western Pacific Ocean and propagates eastward together with the SST >29°C. The period between episodes of westerly wind stress anomaly in the central-eastern Pacific is, as expected, also 5 years.

The time versus longitude model Pacific Ocean SST (degrees Celsius) and τ_x (dynes per square centimeter) diagrams along the equator for RUN2 (weak) are shown in Plates 2a and 2b. They show the same west to east propagation of the highest SST together with the associated zonal convergence field. The exception is a reduction in the ENSO period, where the interval between warm events decreases from 5 to 4.5 years. A characteristic of the simulated SST and τ_x fields for both experiments is the difference in the temporal variability. A strong annual variability is evident in the eastern Pacific Ocean during a cold event but is absent during a warm event. In both simulations the annual cycle is weak or absent in the SST record in the western Pacific Ocean. The difference in sensitivity of the annual cycle between climate epochs and from one side of the basin to the other is explored later where we examine the composites of SST and τ_x.

The model results do not compare favorably with observations because the model produces periodic oscillations. Nonetheless, there are some qualitative resemblance between the two: Figure 3 (Figure 1b from *Kousky and Leetmaa* [1989]) shows a time versus longitude diagram of SST along the equator for an 8-year period from July 1981 to January 1988. In Figure 3 we notice the occurrence of two ENSO episodes. In the first episode, which occurs in 1982–1983, there is eastward propagation of the highest SST, similar to that obtained in Plates 1a and 2a. There is also a second warm episode, in 1986–1987, where there is no obvious eastward propagation associated with it. The interval between these two events is approximately 4–5 years. Like the model results the east Pacific Ocean region in Figure 3 exhibits a more pronounced annual variation during the cold phase, as opposed to the warm phase of ENSO.

The corresponding Indian Ocean time versus longitude distribution of SST (degrees Celsius) along the equator for RUN1 (Plate 3a) and τ_x (dynes per square centimeter) (Plate 3b) presents an entirely different pattern to the one observed in the Pacific Ocean. The main feature of the Indian Ocean is the dominance of the annual cycle, in particular at the western side of the basin. The other characteristic is the moderately weak temperature gradient that is reversed compared to the Pacific Ocean temperature gradient across the basin. The variations in SST introduced by the annual cycle are intimately related with the dynamics of the western boundary Somali current [*Wainer*, 1991]. Lower temperatures are associated with the coastal upwelling that follows the northern hemisphere summer monsoon. During the winter monsoon the upwelling is suppressed, and the temperatures at the western boundary increase. The eastern Indian Ocean temperatures exhibit a weak annual signal, remaining pretty much constant throughout the integration.

There is a distinct change in direction of the zonal wind stress between the northern hemisphere winter and summer monsoons in the western boundary. As we move to the central and eastern Indian Ocean, the annual signal weakens. Of some significance is the variation in intensity of the westerly wind stress anomaly at the very eastern part of the domain. This result will be important at a later stage in establishing a link between the Indian Ocean region and the interannual variability in the Pacific Ocean.

The time versus longitude distributions of model Indian Ocean SST and τ_x along the equator for RUN2 (not shown) present the same spatial structure as in RUN1. The two experiments differ only in magnitude. The two oceans are not allowed to exchange mass, which accounts for the discontinuity observed in the SST distribution at their boundary.

3.1. Time Series

Certainly the most prominent model result is the periodic recurrence of warm events in the Pacific Ocean which are evident from the SST series in Figure 4. The time series are obtained for three subdivisions of the equatorial Pacific Ocean which are marked in Figure 1.

The amplitude of the summer monsoon remains constant throughout RUN1 and RUN2 100-year simulation. The warm events are accompanied by westerly wind stress anomalies and

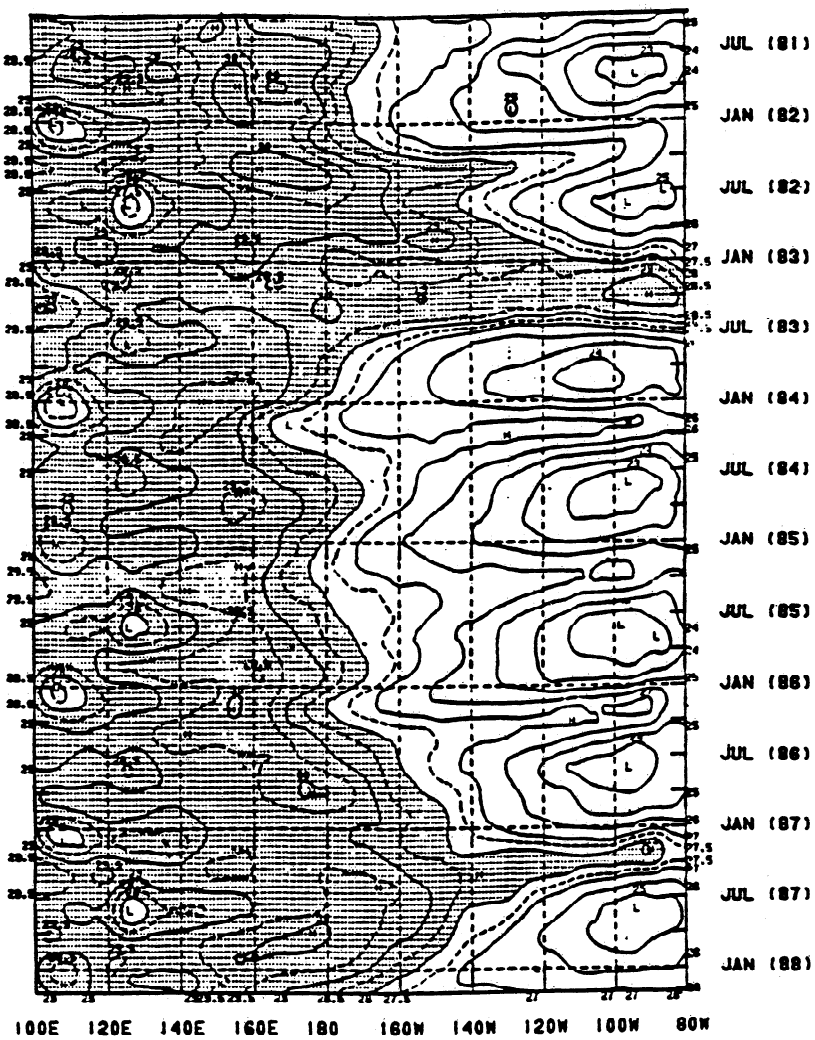

Figure 3. Time versus longitude section of SST (degrees Celsius) averaged between 5°N and 5°S. Regions where SST is greater than 28°C are shaded [from *Kousky and Leetmaa*, 1989].

increased mixed layer depths. Figures 5 and 6 show the time series of the zonal wind stress and mixed layer depth that accompany the SST record. Oscillations between westerly (easterly) wind stress anomaly are in phase with the warming (cooling) of the upper ocean, together with an increase (decrease) in depths.

ENSO cycles are observed in both RUN1 and RUN2. The only difference between them is that the interval between the very regular warm events decreases from 5 to 4.5 years. Though changes in the summer monsoon amplitude appear to be inducing changes in the ENSO period from RUN1 to RUN2, changes in magnitude of the SST (Figure 4) and mixed layer depth (Figure 6) appear small. Changes in magnitude of the τ_x field (Figure 5) are slightly more evident, with higher (lower) values coinciding with the stronger (weaker) monsoon. The longer-period ENSO cycle in this model is linked to stronger monsoons, while the shorter periods are associated with weaker monsoons.

3.2. Composites

Next we discuss the monthly composites of SST and τ_x for the warm and cold years for the strong and the weak monsoon cases. A warm year is defined as the year when the temperature in the eastern Pacific Ocean is greater than 28°C. We concentrate primarily on the zonal structure and time evolution of the fields. The SST fields for RUN1 and RUN2 are presented in Figure 7 for the warm years. The highest temperatures are found in the central Pacific, with the maximum occurring around July–August. Toward the west the temperature decreases with a minimum around September. The temperatures start to increase again with a secondary maximum in the western part of the basin. The annual cycle is not pronounced in any particular region, aside from the occurrence of the maximum and minimum temperatures during the months mentioned above.

The composites of τ_x (not shown) for the warm and cold years are almost mirror images of each other. The warm composites reveal that the eastern side of the Pacific Ocean domain is dominated by westerly wind stress anomaly, which is observed to be associated with warm episodes. The western half is dominated by the easterly wind stress anomaly.

The cold SST composites shown in Figure 8 have a simplified zonal structure. The temperature increases from east to west. Minimum temperatures are found during the northern hemisphere summer months. Maximum temperatures in the western part of the domain remain mostly constant during the

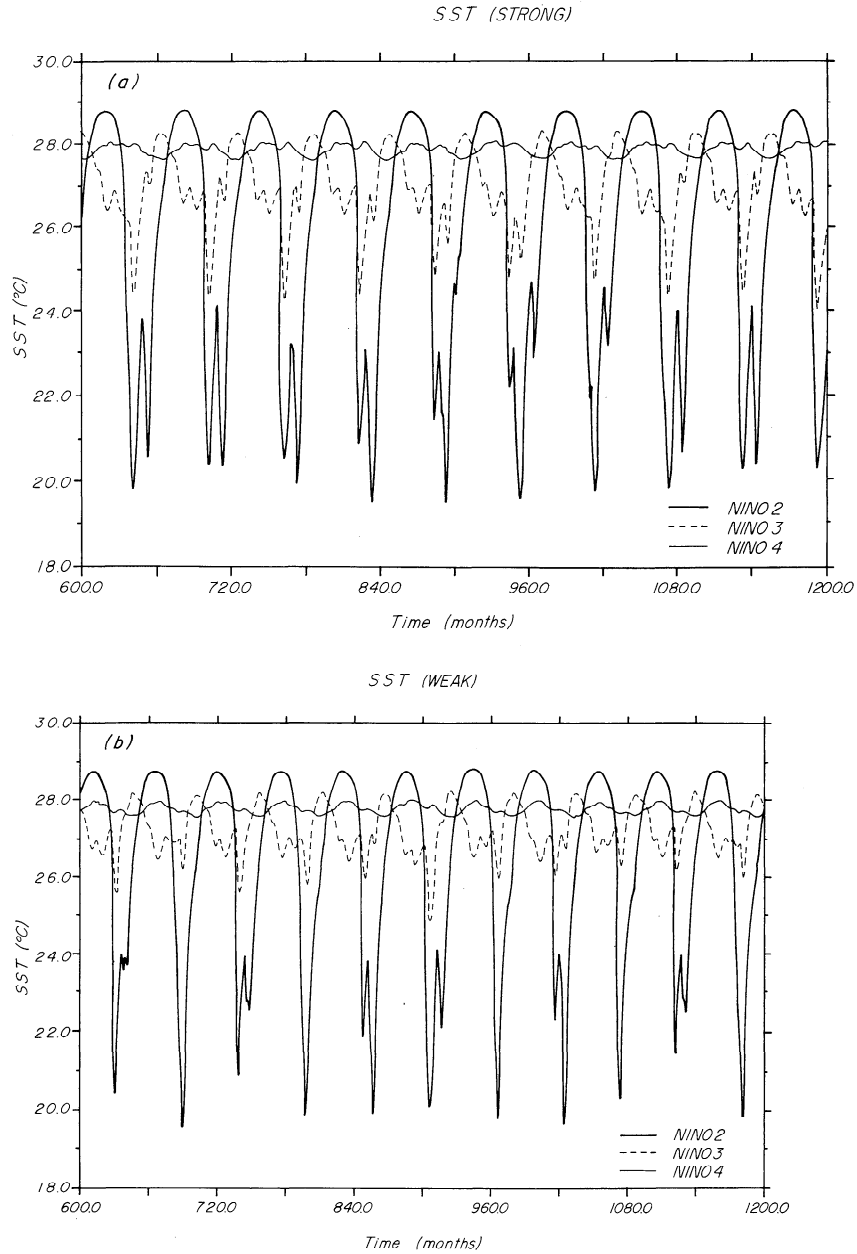

Figure 4. Fifty-year time series for the equatorial Pacific Ocean of SST (degrees Celsius) for (a) RUN1 and (b) RUN2.

entire year. The eastern Pacific is dominated by easterly wind stress anomaly, and the western Pacific is dominated by westerly wind stress anomaly. This is often observed during non-ENSO years.

Looking at the warm and cold composites for the Indian Ocean (Figure 9) for both strong (Figures 9b and 9d) and weak monsoons (Figures 9a and 9c), we see that they are very similar to each other. In this model, ENSO-like interannual variability in the Indian Ocean is quite weak.

3.3. Variable Monsoon

There are two timescales associated with ENSO: the recurrence interval, which we refer to as the ENSO period, and the lifetime of the event itself. The former is irregular, while the latter follows a rather similar evolution lasting anywhere from 18 to 24 months with aspects that are common to all events (e.g., a seasonal timescale weakening of the trade winds and basin scale warming of SST along the equator).

However, throughout much of the 1990s, conditions in the equatorial Pacific suggested the development of a weak ENSO [*McPhaden*, 1993]. Such prolonged warm conditions in the tropical Pacific indicated that the coupled system evolved in a manner unlike that of any event in the recent past for which enough data exist to make reasonable comparisons [cf. *Kousky and Leetmaa*, 1989; *Rasmusson and Carpenter*, 1982].

Significant event-to-event differences challenge attempts to characterize ENSO variability in terms of regularly occurring stages of development. The source of the aperiodicity in the ENSO cycle is still an open question. We believe that the interannual variations in the Pacific Ocean associated with

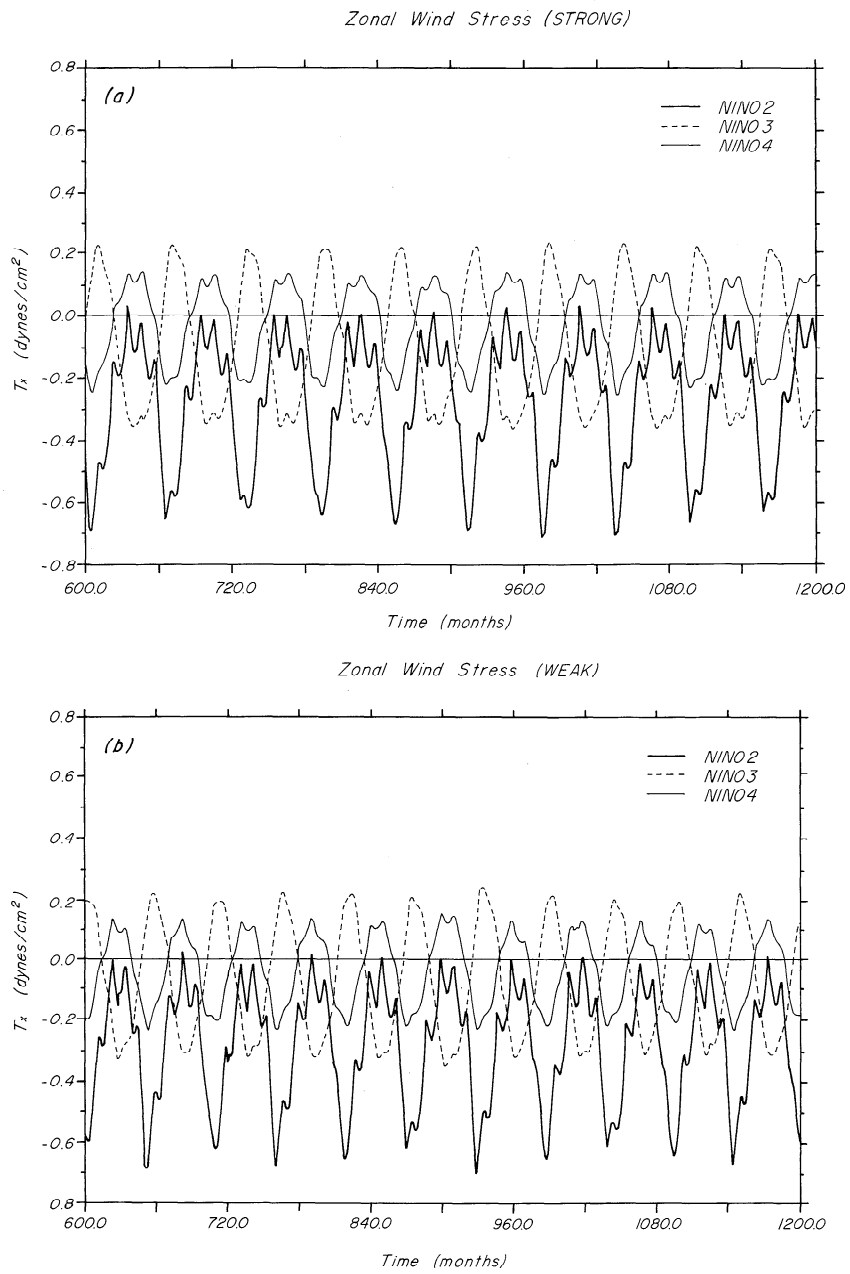

Figure 5. Fifty-year time series for the equatorial Pacific Ocean of τ_x (dynes per square centimeter) for (a) RUN1 and (b) RUN2.

ENSO are closely linked to the interannual variations in the Asian monsoon. To confirm this idea, we next show results from the 100-year simulation for RUN3 (variable monsoon).

The time series presented in Figure 10 for east, west, and central Pacific Ocean indicate that the regular oscillations in the SST (Figure 4), τ_x (Figure 5), and mixed layer depth fields (Figure 6) presented earlier have given place to aperiodic oscillations. Only the last 50 years of the 100-year time series are presented for clarity. The intervals of recurrence of a warm event now vary from 1 to 6 years, depending on the field. To gain a better idea of the timescales associated with the variable monsoon run, we show in Figure 11 the power spectra of the model-derived zonal wind index (U_D) together with the 95% confidence limit curve. This index is calculated by subtracting the equatorial zonal wind at the eastern Pacific Ocean (at 2250 km) from the equatorial zonal wind at the central-western Pacific Ocean (at 9000 km).

The index spectra for RUN1 (Figure 11a) shows only three peak (6, 4–5, 2.5) years, the first and the last barely above the confidence limit curve. The random forcing (Figure 11b) does introduce other timescale (10.5, 6.5, 4–5, 3.5, 2.5) years, but it should be noted that these are very weak and the dominant timescale is still the 4- to 5-year regular cycle.

The differences in the intervals between warm episodes from the variable monsoon experiment can also be seen in the Hovmoller diagram of Pacific Ocean SST (Plate 4a) and τ_x (Plate 4b). Plate 4a shows the west to east propagation of the warm Pacific Ocean SST at irregular interval along the equator. The accompanying regions of zonal convergence along the equator can be seen in Plate 4b. The aperiodic behavior of the model

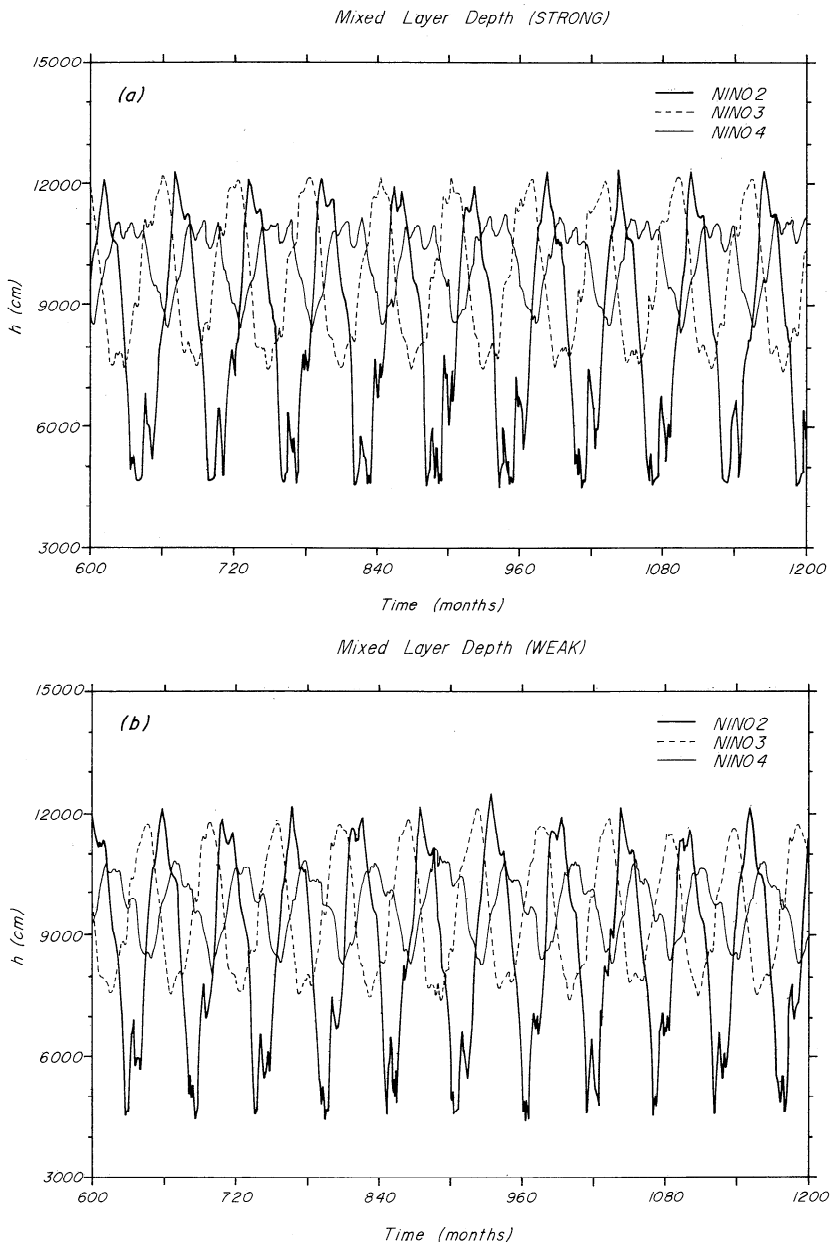

Figure 6. Fifty-year time series for the equatorial Pacific Ocean of mixed layer depth (centimeters) for (a) RUN1 and (b) RUN2.

ENSO cycle leads us to believe that the interannual variability of the monsoon can affect ENSO.

4. Discussion

The Indian and Pacific Oceans respond differently to the annual cycle. The Indian Ocean undergoes a strong annual variation. The amplitude and character of the ocean circulation depend on the annual migration of the monsoon, particularly in the western Indian Ocean. There is a distinct temperature gradient across the basin with higher temperatures in the eastern side decreasing as we move west. Temperatures near the western boundary are modulated by the annual cycle. The most striking characteristic of the equatorial Pacific Ocean, on the other hand, is the regular occurrence of ENSO-like disturbances. The annual cycle is still evident, in particular during the cold phase of ENSO, but the low-frequency structure dominates.

Our results show that the Indian Ocean region is weakly affected by the ENSO-like oscillations in the Pacific Ocean. However, the ENSO cycle is sensitive to changes in the monsoon strength. This motivated the coupling of a stochastic function to the continental heating in order to introduce random interannual variability in the model produced monsoon. When the monsoon is allowed to vary from one summer to the next, aperiodicity in the ENSO cycle appears.

The increase (decrease) of the wind field over the eastern Indian Ocean and central-western Pacific Ocean contributes to the increase (decrease) of the convergence over the western Pacific Ocean. An increase in convergence will produce an increase in the thermocline depth, which implies an increase in

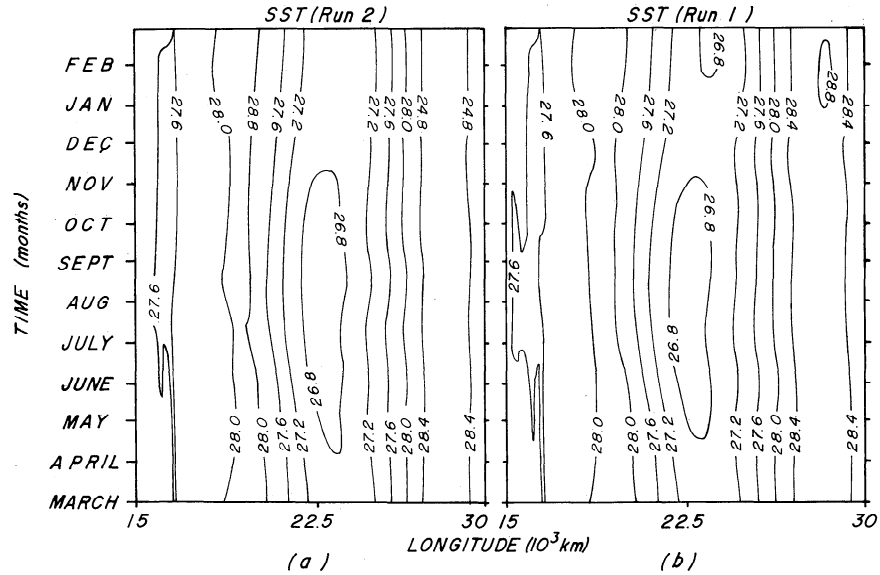

Figure 7. Time-longitude evolution of monthly composites of Pacific Ocean SST (degrees Celsius) for the warm years, along the equator, for (a) RUN2 and (b) RUN1.

the ocean heat content in the western Pacific. Changes in the ocean heat content in the western Pacific will affect the propagation of the coupled ocean-atmosphere disturbance associated with ENSO.

While ENSO is sensitive to changes in the Asian monsoon, the Asian monsoon, being prescribed in this model, cannot be affected by ENSO. We noticed that the SST composites for the Indian Ocean for the warm and cold years are practically identical, which shows that the model's annual cycle in the Indian Ocean is hardly affected by the ENSO variations.

There are several ways in which the model could be improved to better represent ENSO events. Among the most important is the inclusion of a convergence feedback scheme [*Webster*, 1981] as used by *Zebiak and Cane* [1987]. This would relax the condition that SST above a critical level is sufficient to heat the atmosphere. Making the atmospheric heating dependent also on the low-level convergence scheme would yield a more realistic model configuration. Although the model is capable of simulating the basic physical processes associated with the monsoon-ENSO problem, there are some situations that could be improved: (1) The heating over the continent, instead of being externally specified, should be interactive, and (2) if the continental heating is model derived, then the feedback of ENSO with the monsoon could be better tested. This could be an important process for the interannual variation of the monsoon. With this model it is impossible to test this hypothesis.

Many features of the model behavior have been explained only tentatively. However, introducing the suggested modifications, while complicating the model to some extent, would

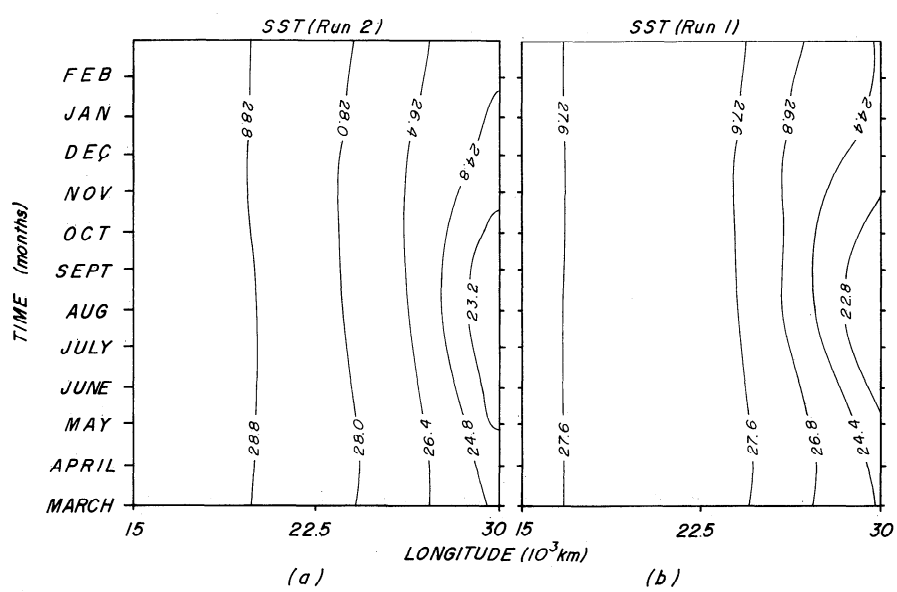

Figure 8. Time-longitude evolution of monthly composites of Pacific Ocean SST (degrees Celsius) for the cold years, along the equator, for (a) RUN2 and (b) RUN1.

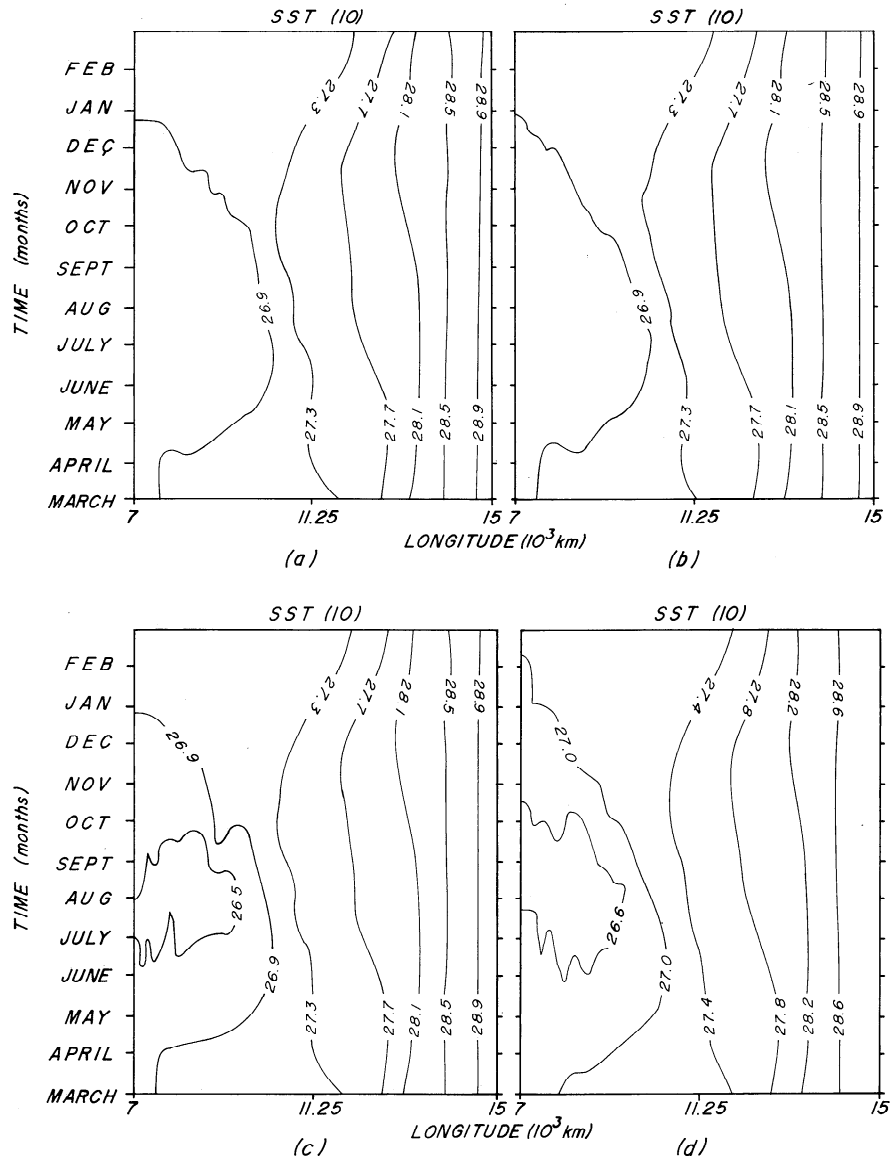

Figure 9. Time-longitude evolution of monthly composites of Indian Ocean SST (degrees Celsius) along the equator for the warm years for (a) RUN2 and (b) RUN1 and for the cold years for (c) RUN2 and (d) RUN1.

allow an even better simulation of the monsoon-ENSO circulation. If so, then further progress may be made in answering the many questions surrounding this intriguing phenomenon.

5. Conclusions

Interannual variability in the Pacific Ocean is produced by a combination of the monsoon variability and the internal dynamics of the coupled ocean-atmosphere system. An example of this self interaction is the feedback argument introduced by *Bjerknes* [1966, 1969], in which the unstable modes are characterized by an initial change in the westward trade winds. The trades tend to pile up warm waters in the western side of the Pacific Ocean basin and expose cold waters on the eastern side. If any changes occur in the winds at the western side of the basin, the changes in the thermocline depth occur. These changes alter the SST distribution that further alters the wind field. This unstable mode travels from the western to the eastern Pacific Ocean. This scenario assumes that the Pacific Ocean is the active part of the coupled ocean-atmosphere system. Our results have shown that the ENSO-like oscillations in the Pacific Ocean are sensitive to the year-to-year changes in the Asian monsoon.

According to the model results, the only interannual variability observed in the Indian Ocean region is associated with the interannual variability of the monsoon itself. This brings us to a very important point: For the ENSO cycle to be fully understood the Indian Ocean-Pacific Ocean sector must be considered. Furthermore, the year-to-year variations in the strength of the summer monsoon appear to be a key ingredient in explaining the aperiodicity of the model's ENSO-like oscillation.

On the basis of the present results it is suggested that no model that ignores the Indian Ocean region can produce realistic ENSO aperiodicity.

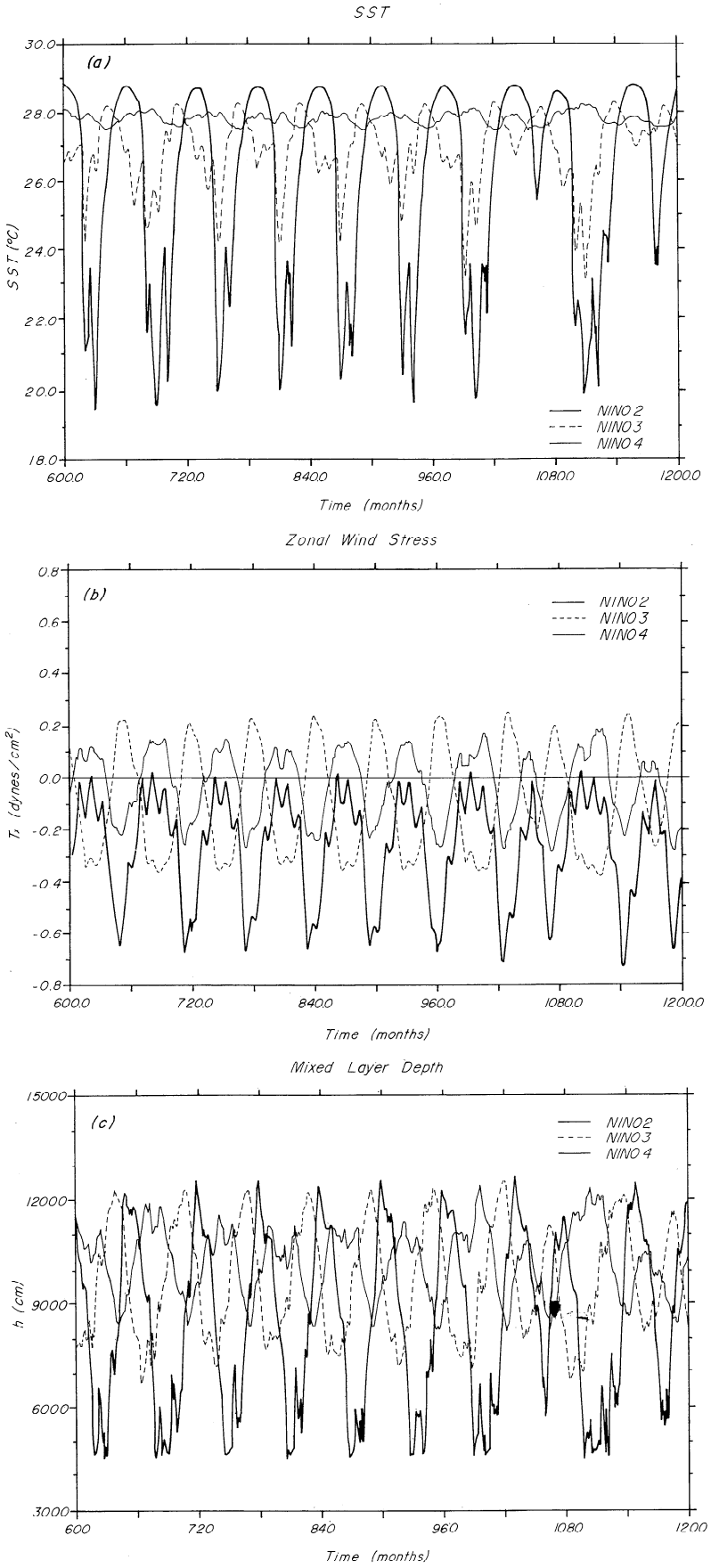

Figure 10. Fifty-year time series for the equatorial Pacific Ocean for RUN3 (variable monsoon) for the three NINO regions (see Figure 1): (a) SST (degrees Celsius), (b) τ_x (dynes per square centimeter), and (c) mixed layer depth (centimeters).

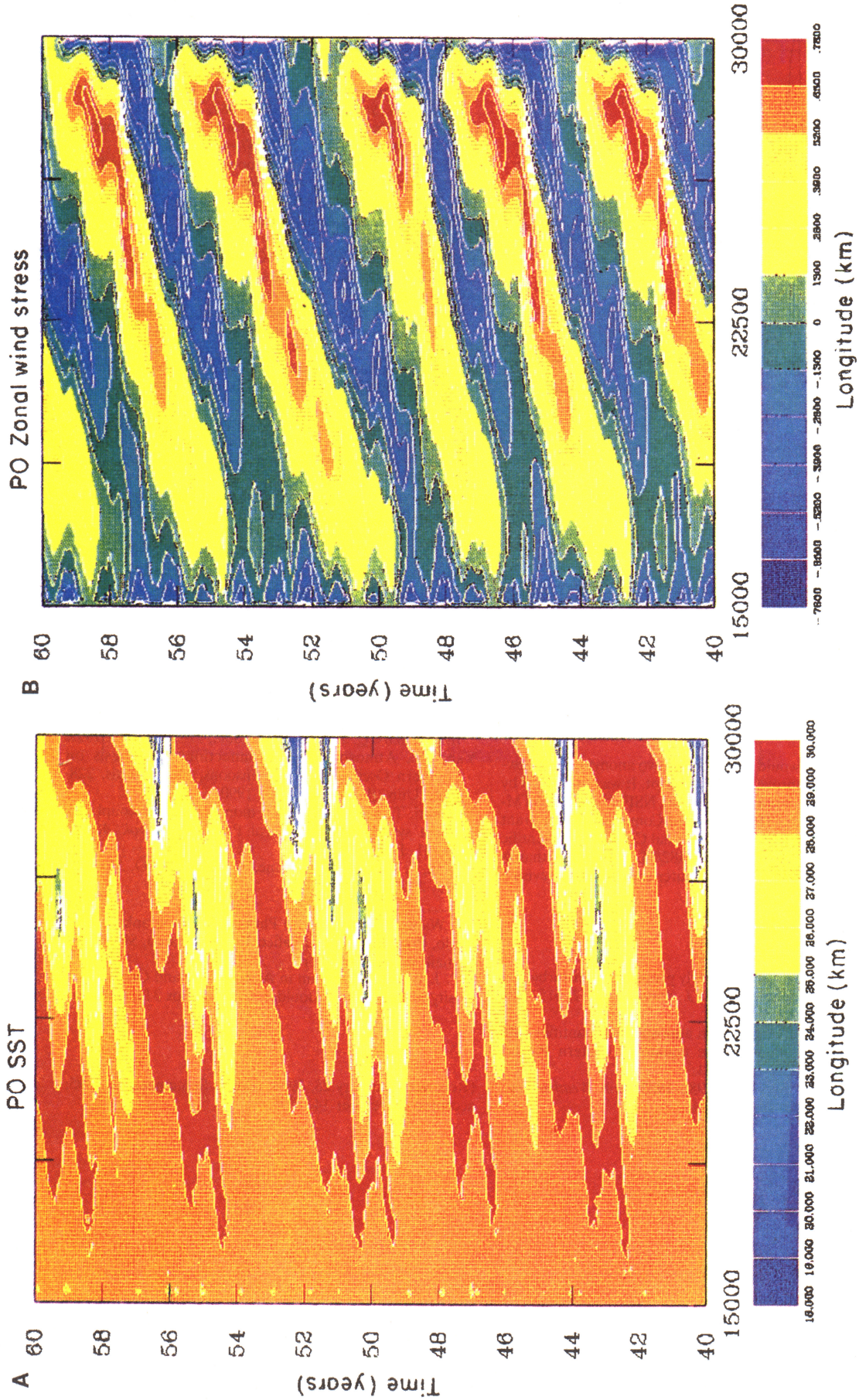

Plate 4. (a) Time versus longitude distribution of the model Pacific Ocean SST (degrees Celsius) along the equator for RUN3. Time goes from the bottom up. The color code on the bottom of the figure has colder temperatures in the blue side of the spectrum. Warmer temperatures are related to the orange-like colors. (b) Time versus longitude distribution of the model Pacific Ocean τ_x (dynes per square centimeter) along the equator for the strong monsoon case. Negative values (easterlies) are in the blue-green side of the spectrum, while positive values (westerlies) lie on the yellow-red side.

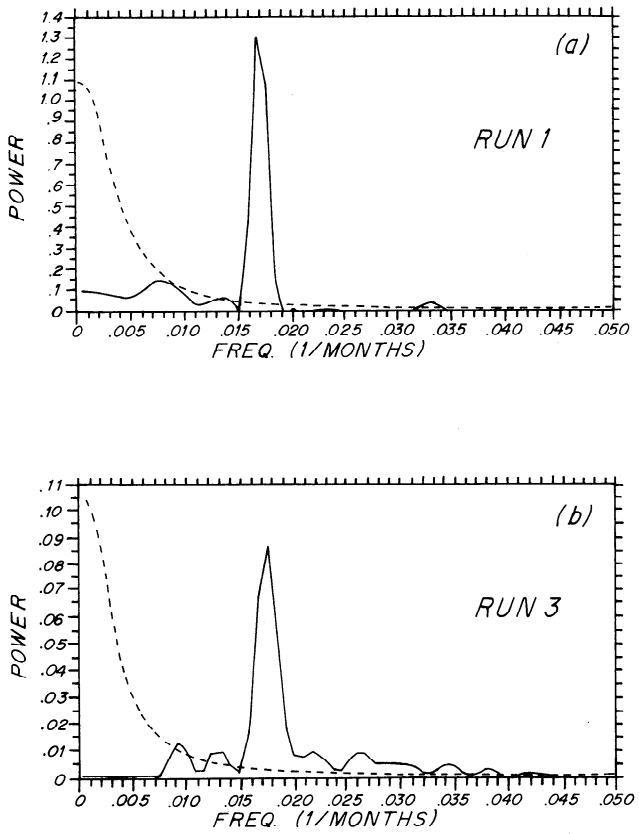

Figure 11. Power spectra and 95% confidence limit curves for the model derived zonal wind index for (a) RUN1 (strong) and (b) RUN3 (variable).

Acknowledgments. We would like to thank two anonymous reviewers for helping to greatly improve this manuscript. It was supported by the National Science Foundation under grant NSF 95-26030, ATM-87-03267, by the United States Department of Commerce under grant NOAA NA89AA-D-AC015, and by the National Council for Scientific Research of Brazil under grant CNPQ 202482/84. The author thanks FAPESP, through grant 93/1387-0 for computer support while revising the manuscript.

References

Anderson, D. L. T., and J. McCreary, Slowly propagating disturbances in a coupled ocean-atmosphere model, *J. Atmos. Sci.*, *42*, 615–629, 1985.

Angell, J. K., Comparison of variations in atmospheric quantities with surface temperature variations in the equatorial eastern Pacific, *Mon. Weather Rev.*, *109*, 230–234, 1981.

Barnett, T. P., Prediction of El Niño of 1982–1983, *Mon. Weather Rev.*, *111*, 756–773, 1984.

Bjerknes, J., A possible response of the atmospheric Hadley circulation to equatorial anomalies of ocean temperature, *Tellus*, *18*, 820–829, 1966.

Bjerknes, J., Atmospheric teleconnections from the equatorial Pacific, *Mon. Weather Rev.*, *97*, 163–172, 1969.

Cane, M. A., and S. E. Zebiak, A theory for El Niño and the Southern Oscillation, *Science*, *228*, 1085–1087, 1987.

Gill, A. E., Some simple solutions for heat-induced tropical circulation, *Q. J. R. Meteorol. Soc.*, *106*, 447–462, 1980.

Haney, R. H., Surface thermal boundary conditions for ocean circulation models, *J. Phys. Oceanogr.*, *1*, 241–248, 1971.

Kousky, V., and A. Leetmaa, The 1986–87 Pacific warm episode: Evolution of oceanic and atmospheric anomaly fields, *J. Clim.*, *2*(3), 254–267, 1989.

McPhaden, M. J., TOGA-TAO and the 1991–93 El Niño–Southern Oscillation Event, *Oceanography*, *6*, 36–44, 1993.

Pant, G. B., and B. Parthasaraty, Some aspects of an association between the Southern Oscillation and Indian summer monsoon, *Arch. Meteorol. Geophys. Bioklimatol. Ser. B*, *29*, 245–252, 1981.

Rasmusson, E. M., and T. H. Carpenter, Variations in tropical sea surface temperature and surface wind fields associated with the Southern Oscillation/El Niño, *Mon. Weather Rev.*, *110*, 354–384, 1982.

Rasmusson, E. M., and T. H. Carpenter, The relationship between eastern equatorial Pacific sea surface temperature and summer monsoon rainfall over India and Sri-Lanka, *Mon. Weather Rev.*, *111*, 517–528, 1983.

Ropelewski, C. F., and M. S. Halpert, Global and regional scale precipitation patterns associated with the El Niño/Southern Oscillation, *Mon. Weather Rev.*, *115*, 1606–1626, 1987.

Shukla, J., and D. Paolino, The Southern Oscillation and long range forecasting of the summer monsoon rainfall over India, *Mon. Weather Rev.*, *111*, 1830–1837, 1983.

Wainer, I., Monsoon-Enso relationships, Ph.D. thesis, 208 pp., Penn. State Univ., University Park, 1991.

Walker, G. T., and E. W. Bliss, World weather IV, *Mem. R. Meteorol. Soc.*, *3*, 81–95, 1930.

Webster, P. J., Mechanisms determining the atmospheric response to SST anomalies, *J. Atmos. Sci.*, *38*, 554–571, 1981.

Webster, P. J., and S. Yang, Monsoon and ENSO: Selectively interactive systems, *Q. J. R. Meteorol. Soc.*, *118*, 877–895, 1992.

Yang, S., Atmospheric teleconnections: Emphasis on El Niño/Southern Oscillation and monsoons, Ph.D. thesis, 228 pp., Penn. State Univ., University Park, 1990.

Yasunari, T., Impact of Indian monsoon on the coupled atmosphere/ocean system in the tropical Pacific, *Meteorol. Atmos. Phys.*, *44*, 29–41, 1990.

Zebiak, S. E., and M. A. Cane, A model ENSO, *Mon. Weather Rev.*, *115*, 2262–2278, 1987.

I. Wainer, Department of Physical Oceanography, University of São Paulo, Praça do Oceanográfico 191, São Paulo, SP-05508-900, Brazil. (e-mail: wainer@usp.br)

P. J. Webster, Program in Atmospheric and Oceanic Sciences, University of Colorado at Boulder, Campus Box 311, Boulder, CO 80309.

(Received February 28, 1994; revised September 12, 1995; accepted November 14, 1995.)